Eur. Phys. J. D **10**, 67–79 (2000)

THE EUROPEAN PHYSICAL JOURNAL D

EDP Sciences

Extracting generalized multiphoton ionization cross-sections from nonperturbative time-dependent calculations: An application in positronium

L.B. Madsen[1,a], L.A.A. Nikolopoulos[2], and P. Lambropoulos[1,2]

[1] Max-Planck-Institut für Quantenoptik, Hans-Kopfermann-Straße 1, 85748 Garching, Germany
[2] Foundation for Research and Technology Hellas, Institute of Electronic Structure and laser, P.O. Box 1527, Heraklion 71110 Crete, Greece

Received 8 June 1999

Abstract. *Ab initio* time-dependent (TD) calculations of the behavior of positronium (Ps) under strong subpicosecond laser pulses are presented. The results are compared with results in H through scaling. It is found that a substantial amount of the population can be found in excited states after the pulse. In the perturbative regime, generalized multiphoton ionization cross-sections are extracted from the results of the time-dependent calculations. The generalized cross-sections are used to predict the response of Ps to nanosecond laser pulses at wavelengths of current experimental interest. Beyond the application to Ps, the generality of the method for extracting generalized cross-sections from TD nonperturbative calculations is discussed.

PACS. 32.80.Rm Multiphoton ionization and excitation to highly excited states (e.g., Rydberg states) – 32.80.-t Photon interactions with atoms – 36.10.Dr Positronium, muonium, muonic atoms and molecules

1 Introduction

It is one of the ironies of multiphoton strong-field theory that the calculation of higher order processes, including above threshold ionization (ATI), is in practical terms easier through time-dependent (TD) nonperturbative techniques than the seemingly straightforward summation in the corresponding transition amplitude of lowest order perturbation theory (LOPT). Although multiphoton ionization cross-sections of hydrogen (H) up to order 16 have been calculated in the past within LOPT [1,2], ATI had not been included and the extension to systems other than H, with the same or similar techniques, is not easy to contemplate. By contrast, ionization spectra including ATI of fairly high order can be and have been calculated in a number of atomic systems through nonperturbative TD techniques; which for appropriately low intensity should provide the LOPT result. But there is a catch. For computational reasons, such calculations are practical only for short pulse durations; say 100 fs or less. Experiments for which LOPT would be appropriate usually correspond to longer pulses; from a few ps to ns. In such situations, one can interpret the results reliably if the cross-sections for the relevant multiphoton processes were known, in which case rate equations representing the relevant channels can be employed. It would thus be extremely useful if one could extract the relevant cross-sections from TD calculations for short pulses.

We were faced with this problem in the course of our recent work on the photobreakup of positronium (Ps) [3–5] and it is one of our purposes in this paper to show how such an approach can indeed be implemented. Since part of this paper is devoted to a detailed study of Ps, we have taken the opportunity to describe the general procedure and then illustrate its practicality through an application to related studies in Ps.

Positronium is the atomic system made up of an electron and its antiparticle the positron. Ps is purely leptonic and therefore particularly interesting for precision quantum electrodynamics measurements and calculations, as it embodies a two-body problem with only electroweak interactions (see, *e.g.*, the reviews of Rich [6] and Mills and Chu [7] and the more recent experiments by Fee *et al.* [8,9]). The gross structure of Ps is determined by the Bohr levels of a charged particle with reduced mass $\mu = m_e/2$ moving in the attractive Coulomb potential, *i.e.*, they are half of those of H. The detailed level structure is understood in terms of fine and hyperfine corrections as well as corrections from virtual annihilation channels. Apart from being an ideal case for spectroscopic tests of quantum electrodynamics, Ps is also of interest in the charge-transfer process with antiprotons, $\mathrm{Ps} + \bar{p} \rightarrow e^- + \bar{\mathrm{H}}$ (see, *e.g.*, the recent review by Holzscheiter and Charlton [10] and references therein). This process is a promising candidate for the

[a] e-mail: lam@ipp.mpg.de

production of *cold* as opposed to energetic antihydrogen which was produced recently by high-energy antiproton-nucleus collisions at CERN [11] and Fermilab [12].

Our interest in Ps stems from ongoing experimental activities at the Aarhus Positron Beamline aiming at a study of the strong field driving and photobreakup of Ps in laser fields [13]. In the course of our investigations, we have reported on surprisingly high few-photon excitation probabilities of Ps under intense laser pulses of durations in the subpicosecond regime [4]. The excitation by pulses of such a short duration is instantaneous on the timescale of annihilation since the lifetimes of the singlet and triplet ground states are $\tau_{\rm sing} = 1.25 \times 10^{-10}$ and $\tau_{\rm trip} = 1.4 \times 10^{-7}$ s, respectively. The lifetime of excited s-states increases in proportion to n^3 and states with non-zero angular momentum are even more stable against annihilation [14]. In fact, these states will decay by annihilation after their eventual radiative decay to the ground state. Also, with respect to radiative decay, the excitation by subpicosecond pulses may be considered instantaneous since the typical lifetime is $\tau_{\rm rad}^{\rm (Ps)} = 2\tau_{\rm rad}^{\rm (H)} \sim 10^{-8}$ s, where the factor of two comes from scaling [3]. First, this makes it possible to study spectroscopy of excited states trough the entire radiative lifetime. Second, the cross-section for the charge-transfer process, $\mathrm{Ps} + \bar{p} \rightarrow e^- + \bar{\mathrm{H}}$, increases rapidly with the excitation of Ps [15]. This may provide an effective excitation mechanism in connection with the possible production of cold antihydrogen. The excitation by pulses of short duration is effective over a broad range of intensities making it insensitive to focusing and volume effects. In this paper, we extend the study of "instantaneous" excitation to a wider selection of frequencies entering the regimes where 5 and 6 photons are need to ionize Ps.

We have recently considered general scaling properties of hydrogenic systems interacting with laser fields [3]. The problem of the reduced mass particle of the Ps atom interacting with a laser field scales with the corresponding problem for any two-body Coulomb system. However, the behavior of the true particles is very different. Whereas in the photobreakup of an ordinary atomic system, the electron carries essentially all of the energy absorbed from the radiation field, the electron-positron pair shares this energy and both fly apart. One immediate consequence is that the separation in energy between adjacent peaks in the photoelectron energy spectrum in the center of mass system with Ps initially at rest is not the photon energy, $\hbar\omega$, but only half, $\hbar\omega/2$. This effect is apparent in the figures below showing the photoelectron energy spectrum. Note in passing, that the observation of the energy sharing does not require the absorption of excess photons, since already the lowest order ionization channel carries that information. Scaling laws [3] make it possible to calculate generalized cross-sections for Ps from accurate existing values for H [1,2]. This procedure, however, allows the study of the photobreakup process only in the perturbative regime. In the nonperturbative regime, the discussion in reference [3], based on the scaling of the time-dependent Schrödinger equation (TDSE), shows that, at scaled frequencies and pulse durations, Ps breaks up at an intensity 16 times lower than H does. That information alone, however, does not reveal the behavior of non-linear processes. In the present paper, we present nonperturbative TD calculations of Ps under intense 50 fs pulses. In particular, we focus at laser wavelengths which are available in the ongoing Aarhus experiment and which correspond to the two-, three-, and six-photon ionization regimes [13]. We present ionization yields and photoelectron energy spectra. In the perturbative regime, we extract generalized cross-sections for the N-photon ionization process as well as for $(N + S)$-photon ionization processes, where S denotes the number of photons absorbed above threshold. The method, for obtaining these generalized cross-sections, is generally valid for any atomic or molecular system. Finally, the generalized cross-sections are used to predict photoelectron spectra for the nanosecond pulses used in the Aarhus experiment [13].

We describe the system by the non-relativistic Schrödinger equation. Even on the timescale of a nanosecond pulse, the annihilation of the triplet state can be neglected. The electric dipole interaction of the laser does not mix the singlet and triplet manifolds and calculations for any of the two carry over to the other. In realistic experimental situations, the singlet component will decay on its way to the interaction region.

2 Method of calculation

The computational procedure for the representation of the atomic orbitals used here has been presented in detail in references [16,17] for the case of hydrogenlike atoms. For completeness, we include a summary of the method in this section (see also the recent review of Lambropoulos *et al.* [18] and references therein). Exploiting the spherical symmetry of the Coulomb interaction, the orbitals are described by the values of their principal (n), angular (l) and magnetic (m) quantum numbers, and are written as,

$$\phi_{nlm}(\mathbf{r}) = \frac{P_{nl}(r)}{r} Y_{lm}(\theta, \phi), \tag{1}$$

where the radial functions $P_{nl}(r)$ satisfy

$$\left[\frac{\mathrm{d}^2}{\mathrm{d}r^2} + \frac{2\mu}{\hbar^2}(E_{nl} + \frac{Ze^2}{r}) - \frac{l(l+1)}{r^2}\right] P_{nl}(r) = 0, \tag{2}$$

with E_{nl} being the eigenvalue. Hydrogenlike ions or atoms are represented by assigning appropriate values to the nuclear charge, Z, and the reduced mass, μ. The P_{nl} functions with negative or positive eigenvalues are expanded on a set of B-splines of order k and total number q defined in the finite interval $[0, R]$. In the present case, $k = 9$ with $q = 600$ and $R = 900a_0$. The knot sequence that we use is uniform through the finite interval. This ensures a good description of both the bound and the (discretized) continuum states.

Having obtained the eigenstates of the unperturbed atom for each angular momentum, we study its interaction with the laser field as follows. The TDSE for the atom

(the reduced mass particle) in an external laser field is written as,

$$\mathrm{i}\hbar\partial_t\psi(\mathbf{r},t) = [H_0 + V(t)]\ \psi(\mathbf{r},t) \tag{3}$$

with H_0 the free-field Hamiltonian and $V(t)$ the TD interaction between the atom and the laser field. In the velocity gauge and in the dipole approximation, the interaction operator is

$$V(t) = \frac{-\mathrm{i}\hbar e}{\mu c}\mathbf{A}(t)\boldsymbol{\nabla}, \tag{4}$$

with $\mathbf{A}(t)$ being the vector potential which is connected with the electric field through the relation $\mathbf{E}(t) = -c^{-1}\partial_t\mathbf{A}(t)$. In our calculations, we assume laser fields linearly polarized along the z-axis for which,

$$\mathbf{A}(t) = \mathbf{e}_z\, A_0\, g(t)\, \sin\omega t, \tag{5}$$

where

$$g(t) = \sin^2(\pi t/T) \tag{6}$$

is the pulse envelope of duration T. This particular envelope is used for computational convenience and is known to produce results very similar to the ones obtained with the slightly more realistic Gaussian envelope. Notice, that the TD Hamiltonian is invariant with respect to rotations about the z-axis. Therefore, the magnetic quantum number is conserved. The expansion of the TD wave function in the basis $\{\phi_{nl}\}$ now reads

$$\psi(\mathbf{r},t) = \sum_{n,l} b_{nl}(t)\,\phi_{nl}(\mathbf{r}). \tag{7}$$

Substitution into equation (3) provides a system of coupled first-order differential equations for the unknown coefficients $b_{nl}(t)$:

$$\mathrm{i}\hbar\partial_t b_{n,l} = \sum_{n',l'} \left(E_{nl}\,\delta_{nn'}\delta_{ll'} + \langle\phi_{nl}|V(t)|\phi_{n'l'}\rangle\right) b_{n'l'}\ , \tag{8}$$

which is solved subject to the initial condition,

$$|b_{n=1,l=0}(t=0)|^2 = 1.$$

Propagating equation (8) until the end of the pulse, we calculate the ionization probability (P) and the the photoelectron energy spectrum ($\mathrm{d}P/\mathrm{d}E$) through the relations [19],

$$P(t\sim\infty) = \sum_{l,n(E\geq 0)} |b_{l,n(E)}(t\sim\infty)|^2, \tag{9}$$

$$\frac{\mathrm{d}P}{\mathrm{d}E}(E_\mathrm{c}, t\sim\infty) = \sum_{l,n(E=E_\mathrm{c})} |b_{l,n(E)}(t\sim\infty)|^2. \tag{10}$$

Conventional lowest-order perturbation theory gives the ionization rate $\Gamma^{(N)}$ of an N-photon process as the product of the generalized cross-section $\hat{\sigma}_N$ of the process and the Nth power of the flux F of the field, *i.e.* $\Gamma^{(N)} = \hat{\sigma}_N F^N$. This relation, however, is valid when no significant amount of ionization or excitation takes place during the rise of the pulse. On the other hand, nonperturbative TD methods have the time-dependent nature of the laser field inherent in their formalism, and a direct comparison with strong-field experiments (where the laser field has a pulsed shape) is possible. Nevertheless, in the limit of low intensities the results of the TD methods, should be identical with those obtained by perturbative approaches. This is discussed in detail in Section 4.

The figures below show results of our TD calculations. The basis that we have used has been checked for convergence with variations in box radius and in the number of B-splines. Specifically, the quality of the basis has been checked through comparison with published results in H [20]. The ionization yields in Figure 5 of reference [20] have been reproduced with the hydrogenic basis, and also with the basis for Ps at scaled laser intensities, pulse duration and photon energy (see Sect. 3 and Ref. [3]). Similarly, the photoelectron energy spectra have been compared with results in reference [20] and the agreement is good. Typically, we have used angular momenta up to $l = 14$ for the higher order processes ($N = 5{-}6$), while $9{-}10$ angular momenta where sufficient for the low-order processes ($N = 2{-}3$).

3 Scaling

It is important to understand the rules behind universal scaling properties in a particular physical problem in order to avoid redundancies in measurement and analysis of data so as to extract genuine physical effects from the data [3,21]. In this section, we summarize some of the results on scaling which we will need later. In reference [3] the TDSE of any hydrogenlike system of reduced mass μ and charge Z, in the following denoted by A, interacting with an electromagnetic field was shown to scale with the corresponding equation for H. It was found, that length (s) and time (t) scale according to

$$s^{(\mathrm{A})} = \left(\frac{a}{a_0}\right) s^{(\mathrm{H})}, \tag{11}$$

$$t^{(\mathrm{A})} = \left(\frac{E_\infty^{(\mathrm{H})}}{E_\infty^{(\mathrm{A})}}\right) t^{(\mathrm{H})}, \tag{12}$$

where a_0 is the Bohr radius and $a = (m_\mathrm{e}/\mu)a_0/Z$ while $E_\infty^{(\mathrm{H})}$ and $E_\infty^{(\mathrm{A})}$ are the ionization potentials of H and A. It was also found, that field strength ($\mathcal{E}_0$) and frequency and energy (ω) scale as

$$\mathcal{E}_0^{(\mathrm{A})} = \left(\frac{a_0}{a}\right)^2 Z\mathcal{E}_0^{(\mathrm{H})} \tag{13}$$

$$\omega^{(\mathrm{A})} = \left(\frac{E_\infty^{(\mathrm{A})}}{E_\infty^{(\mathrm{H})}}\right)\omega^{(\mathrm{H})}. \tag{14}$$

The pulse duration scales according to equation (12). This ensures that the number of laser cycles experienced by A and H is equal.

From the above equations, we readily derive the following relation between ionization probabilities

$$P^{(\mathrm{A})}\left(\mathcal{E}_0,\omega,T\right) = P^{(\mathrm{H})}\left(\frac{\mathcal{E}_0}{(a_0/a)^2 Z},\frac{\omega}{(E_\infty^{(\mathrm{A})}/E_\infty^{(\mathrm{H})})},\frac{T}{(E_\infty^{(\mathrm{H})}/E_\infty^{(\mathrm{A})})}\right). \quad (15)$$

This equation simply connects the total ionization probability of the (μ, Z) system to that of H at the end of the pulse of duration T at scaled quantities as indicated. Equation (15) shows, *e.g.*, that the ionization yield for N-photon ionization of He^+ may be obtained from that of H at an intensity 2^6 times larger and for a pulse 2^2 times shorter, at the appropriately scaled frequency. Interestingly, equation (15) also allows a discussion of the scaling behavior under an intense laser field of exotic atomic systems as Ps ($\mu = 1/2$, $Z = 1$).

The scaling of the photoelectron spectrum, including above threshold ionization (ATI), follows from equation (15) and the scaling of the energy in equation (14)

$$\frac{\mathrm{d}P^{(\mathrm{A})}}{\mathrm{d}E^{(\mathrm{A})}}\left(\mathcal{E}_0,\omega,T\right) = \left(\frac{E_\infty^{(\mathrm{H})}}{E_\infty^{(\mathrm{A})}}\right) \times \frac{\mathrm{d}P^{(\mathrm{H})}}{\mathrm{d}E^{(\mathrm{H})}}\left(\frac{\mathcal{E}_0}{(a_0/a)^2 Z},\frac{\omega}{(E_\infty^{(\mathrm{A})}/E_\infty^{(\mathrm{H})})},\frac{T}{(E_\infty^{(\mathrm{H})}/E_\infty^{(\mathrm{A})})}\right). \quad (16)$$

Relations (15, 16) may be used to decrease the number of hydrogenlike species one has to investigate in order to get a complete picture of the ionization dynamics of Coulombic one-electron systems. This is the essence of scaling.

Note that the ratios a/a_0 and $E_\infty^{(\mathrm{A})}/E_\infty^{(\mathrm{H})}$ can be expressed in terms of the nuclear charge Z, the electron mass m_e and the reduced mass μ in the case of hydrogenlike systems. We have, however, kept the ratios between characteristic length and energy dimensions since the scaling laws then naturally translate into (and confirm) the semiempirical scaling laws for arbitrary atoms derived some time ago [22].

In the perturbative regime (LOPT), we may extract the dependence on the field strength and the intensity I from equations (15, 16). If we use equation (20) of reference [3] we find

$$P^{(\mathrm{A})}_{\mathrm{LOPT}}\left(\omega\right) = \left(\frac{a^2}{a_0^2}\right)^N \left(\frac{E_\infty^{(\mathrm{H})}}{E_\infty^{(A)}}\right)^{2N-1} \frac{T^{(\mathrm{A})}}{T^{(\mathrm{H})}} \left(\frac{I^{(\mathrm{A})}}{I^{(\mathrm{H})}}\right)^N \times P^{(\mathrm{H})}_{\mathrm{LOPT}}\left(\frac{\omega}{(E_\infty^{(\mathrm{A})}/E_\infty^{(\mathrm{H})})}\right) \quad (17)$$

for the total ionization probability (yield) and

$$\frac{\mathrm{d}P^{(\mathrm{A})}_{\mathrm{LOPT}}}{\mathrm{d}E^{(\mathrm{A})}}\left(\omega\right) = \left(\frac{a^2}{a_0^2}\frac{{E_\infty^{(\mathrm{H})}}^2}{{E_\infty^{(\mathrm{A})}}^2}\right)^{N+S} \frac{T^{(\mathrm{A})}}{T^{(\mathrm{H})}} \left(\frac{I^{(\mathrm{A})}}{I^{(\mathrm{H})}}\right)^{N+S} \times \frac{\mathrm{d}P^{(\mathrm{H})}_{\mathrm{LOPT}}}{\mathrm{d}E^{(\mathrm{H})}}\left(\frac{\omega}{(E_\infty^{(\mathrm{A})}/E_\infty^{(\mathrm{H})})}\right), \quad (18)$$

for the individual peaks $S = 0, 1, 2, \ldots$ in the photoelectron energy spectrum. In equations (17, 18) we have not scaled the pulse durations. For a given order, N, equations (17, 18) show that the signal scales with the atomic size and inversely with the ionization potential. In the limit $N \gg 1$, the scaling procedure for arbitrary atoms introduced in reference [22] in fact leads to the same result. In the perturbative regime, we see from equation (17) that *only one* curve characterizes the ionization yield as a function of intensity, pulse duration and across the isoelectronic sequence of H. The ionization yield for a particular hydrogenlike element and a particular pulse duration is obtained from this universal curve by a simple rescaling of the intensity. Explicitly, to obtain the same yield in two different elements subject to pulses of equal durations but scaled frequencies the intensity should be scaled according to

$$I^{(\mathrm{A})} = I^{(\mathrm{H})}\left(a^2/a_0^2\right)\left(E_\infty^{(\mathrm{H})}/E_\infty^{(\mathrm{A})}\right)^{2-1/N}.$$

If, for a specific element, one considers changes in the pulse duration by a multiplicative constant α the two combinations of intensity and pulse duration $(I, \alpha T)$ and $(\alpha^{1/N} I, T)$ give equal yields. This result applies, in particular, to the scaling of the saturation intensity with pulse duration: a shorter pulse gives rise to a higher saturation intensity. If T is decreased, the ionization yield curve will eventually enter a regime of intensities where the $S \neq 0$ channels are comparable to the $S = 0$ channel and the universality of the ionization yield curve is broken. For a fixed yield, we note that the (saturation) intensity is much more sensitive to variations in the pulse length for a process of a low than of a higher order.

We note that equation (17) predicts the ion yield from Ps to be 2^{4N} times larger than in H for the N-photon ionization process at scaled pulse duration and frequency but at equal intensities. Similarly, equation (18) shows that a photoelectron energy peak corresponding to the breakup of Ps by the absorption of $N + S$ photons is $2^{4(N+S)+1}$ times higher than the corresponding peak in H. This leads to significant enhancement factors. For example, in the six-photon ionization regime, the second ATI peak ($N + 1 = 7$) is $2^{29} \approx 5.4 \times 10^8$ times larger than in H in the perturbative regime.

4 Rate equations

In the first part of this section, we summarize a dynamical model for the calculation of ATI spectra in LOPT.

The model involves the solution of rate equations and requires the knowledge of generalized cross-sections. In the second part of the section, we give a general prescription for extracting values of the generalized cross-sections from TD nonperturbative calculations.

4.1 Calculating ATI spectra in LOPT

Let N_0 be the initial number of neutral atoms in the interaction region. Normalizing the number of neutrals and ions during the pulse to this initial number we have the number (probability) conservation condition

$$n(t) = 1 - n^+(t) = 1 - \sum_S n_S^+(t). \tag{19}$$

Within LOPT the rate of change of the neutrals is given by

$$\frac{\mathrm{d}}{\mathrm{d}t} n(t) = -\sum_S \hat{\sigma}_{N+S} F^{N+S}(t) n(t) \tag{20}$$

and the differential equations for the different photon absorption channels are

$$\frac{\mathrm{d}}{\mathrm{d}t} n_S^+(t) = \hat{\sigma}_{N+S} F^{N+S}(t) n(t), \quad S = 0, 1, 2, \ldots, \tag{21}$$

with $\hat{\sigma}_{N+S}$ the generalized cross-section for an ionization process in which S photons are absorbed above the N-photon ionization threshold. In practice, of course, the summation in equation (20) has to be truncated at a value of S above which the contribution to the ionization process is negligible. This cut-off value depends on the intensity, the duration of the pulse and the order of non-linearity vis-a-vis experimental sensitivity. As N increases, the number of channels we need to include increases as low energy photons are more easily absorbed in the continuum than photons of larger energy. Denoting the peak value of the photon flux by F_0, the time-dependent flux is given by $F(t) = F_0 f(t)$, where $f(t)$ describes the temporal evolution of the pulse. Photon flux is the number of photons per cm^2 per second and is connected to the intensity in $\mathrm{W/cm}^2$ *via*

$$F\left[\frac{1}{\mathrm{cm^2 s}}\right] = \frac{0.624 \times 10^{19}}{\hbar\omega[\mathrm{eV}]} I[\mathrm{W/cm^2}]. \tag{22}$$

The generalized cross-section of order N is measured in units of $\mathrm{cm}^{2N}\mathrm{s}^{N-1}$.

The solutions to equations (20, 21) with the initial conditions $n(0) = 1$ and $n_S^+(0) = 0$ ($S = 0, 1, 2, \ldots$) are

$$n(t) = \exp\left(-\sum_S \hat{\sigma}_{N+S} F_0^{N+S} T_{\mathrm{eff}}^{(N+S)}(t)\right) \tag{23}$$

$$n_S^+(t) = \int_0^t \mathrm{d}t' \hat{\sigma}_{N+S} F(t')^{N+S} n(t'), \quad S = 0, 1, 2, \ldots \tag{24}$$

where we have introduced the time

$$T_{\mathrm{eff}}^{(M)}(t) = \int_0^t f(t')^M \mathrm{d}t', \tag{25}$$

which gives the effective interaction time at $t \sim \infty$, to be understood as the overall time of the atom-light interaction for a process of order M. These equations show that within LOPT the different ionization channels couple only to the ground state and not to each other. Population left in excited states is not accounted for in this model. If necessary, this can be incorporated by increasing the number of equations. The quantity $n^+(t \sim \infty) = 1 - n(t \sim \infty)$, mapped versus intensity, gives the ionization yield as a function of intensity. The quantities $n_S^+(t \sim \infty)$ give the number of ions in the different channels ($S = 0, 1, 2, \ldots$) and constitute the photoelectron energy spectrum.

Below, we present results of equations (23, 24) for nanosecond pulses at wavelengths of experimental interest. The main theoretical input into equations (23, 24) are the values of the generalized cross-sections. Their calculation requires a good representation of bound and continuum states and the computational task increases significantly with the order of non-linearity. Nevertheless, accurate values for H have existed for some time at a selection of wavelengths [1,2], even for generalized cross-sections involving excess photon absorption [23,24]. The generalized cross-sections for Ps (or any other hydrogen-like system) of the same order N can be obtained by scaling [3]. Often, however, the generalized cross-sections are not available at the (scaled) wavelengths of interest. The question then arises, if it is possible to extract accurate generalized cross-sections, including the ones describing ATI, from a nonperturbative TD calculation which would be applicable to any atom. As discussed below, this is indeed possible.

4.2 Extracting generalized cross-sections from nonperturbative time-dependent calculations

At sufficiently low intensity the ionization yield is small corresponding to an insignificant change in the number of neutrals during the pulse, $n(\infty) \approx n(0) = 1$. The set of equations in equation (24) then simplifies to ($S = 0, 1, 2, \ldots$)

$$n_S^+(t) = \hat{\sigma}_{N+S} F_0^{N+S} T_{\mathrm{eff}}^{(N+S)}(t), \tag{26}$$

which describes a situation where depletion is neglected.

The result of a nonperturbative calculation performed in the low intensity regime may be used to extract values of the generalized cross-sections. In our TD calculation we used the $\sin^2$-pulse envelope of equation (6) for the field which gives a $\sin^4$ intensity profile. For an M-photon process, the effective interaction time corresponding to a pulse of length T is thus determined by [25]

$$T_{\mathrm{eff}}^{(M)} = \int_0^T \mathrm{d}t \sin^{4M}\left(\frac{\pi t}{T}\right) = \frac{(4M-1)!!}{(4M)!!} T, \tag{27}$$

which is a decreasing function of the order of the process. For a given pulselength, T, which is short enough to make a time-propagation of the TDSE practically possible, say below 100 fs, the photoelectron spectrum and knowledge

Table 1. Excess energies, ΔE, and ponderomotive shifts, $U_{\rm P}$, in eV and Keldysh parameters, $\gamma = \sqrt{E_\infty/(2U_{\rm P})}$, for Ps and H in the two-, three-, five- and six-photon ionization cases, corresponding to wavelengths of 355, 532, 780, and 1064 nm for Ps and 177.5, 266, 390, and 532 nm for H, respectively. The intensity, I, is measured in W/cm^2.

N	$\Delta E^{(\rm Ps)}$	$\Delta E^{(\rm H)}$	$U_{\rm P}^{(\rm Ps)}$	$U_{\rm P}^{(\rm H)}$	$\gamma_{\rm Ps}$	$\gamma_{\rm H}$
2	0.18	0.37	$\frac{I}{4.25\times10^{13}}$	$\frac{I}{3.40\times10^{14}}$	$\sqrt{\frac{1.45\times10^{14}}{I}}$	$\sqrt{\frac{2.31\times10^{15}}{I}}$
3	0.19	0.38	$\frac{I}{1.89\times10^{13}}$	$\frac{I}{1.51\times10^{14}}$	$\sqrt{\frac{6.43\times10^{13}}{I}}$	$\sqrt{\frac{1.03\times10^{15}}{I}}$
5	1.15	2.30	$\frac{I}{8.88\times10^{12}}$	$\frac{I}{7.04\times10^{13}}$	$\sqrt{\frac{3.02\times10^{13}}{I}}$	$\sqrt{\frac{4.79\times10^{14}}{I}}$
6	0.19	0.38	$\frac{I}{4.73\times10^{12}}$	$\frac{I}{3.78\times10^{13}}$	$\sqrt{\frac{1.61\times10^{13}}{I}}$	$\sqrt{\frac{2.57\times10^{14}}{I}}$

of the total ionization yield provide the left-hand side of equation (26) by normalizing the height (area) of the Mth peak to the sum of the heights (areas) of the ATI peaks and multiplying by the total ionization yield (in practice $\sim 10^{-4}$–10^{-3}). On the right-hand side, the only unknown quantity is the generalized cross-section. In Table 2, we show some values of generalized cross-sections determined in this way. Since depletion is neglected the resulting values of the generalized cross-section should be lower estimates of the true values. When possible, we have compared with values available in the literature and the agreement is good [1,2]. From our experience with this procedure for the calculation of the generalized cross-sections, we conclude that the value of the generalized cross-section for $S_{\rm max}$ for each N is a low and uncertain estimate. This is because this outer-most peak is not very significant compared with the background signal of the photoelectron energy spectrum. If we want to take the depletion of the ground state during the pulse into account, we need to calculate the ionization yield at appropriate time steps during the pulse. This approach has not been considered in the present work. Notice that, for a fixed intensity, being in the perturbative regime with a pulse of short duration automatically ensures the validity of perturbation theory for a pulse of a longer duration. In this respect, the breakdown of LOPT is not related to the ionization yield but to the question of whether any atom will be stable against ionization during the rise of the pulse as to experience the peak intensity and therefore react to the field in a nonperturbative way. Of course, a much smaller number of atoms will do so for pulses of long than short duration.

A slight complication arises if the ponderomotive shift, which gives the shift of the threshold and is equal to the quiver energy of a free charged particle in the laser field,

$$U_{\rm P}[\text{a.u.}] = \frac{I[\text{a.u.}]}{4\mu[\text{a.u.}]\omega^2[\text{a.u.}]} \tag{28}$$

is already, in the otherwise perturbative regime, large enough to cause a closing of the lowest ionization channel. This happens for processes of a rather high-order (low photon energy) and in cases when the N-photon absorption places the electron (reduced mass particle) just above the threshold with a small excess energy, ΔE. In our case for Ps, we are confronted with such a situation in the six-photon ionization regime for the wavelength of 1064 nm (see Tab. 1 with the ponderomotive shifts and the Keldysh parameters). Taking into account the time-dependent shift of the threshold $U_{\rm P}(t)$, the $S=0$ channel closes if $U_{\rm P}(t) > \Delta E$ for some time t during the pulse. This fixes the critical intensity $I_{\rm cr}$ and thus the critical time $t_{\rm cr}$ during the pulse envelope at which the channel closes $t_{\rm cr} = (T/\pi)\sin^{-1}[(I_{\rm cr}/I_0)^{1/4}]$, where we have used the $\sin^4$ intensity profile. In the case of a channel closing, the flux is given by $F(t) = 0$ for $t \in [t_{\rm cr}, T - t_{\rm cr}]$ and $F(t) = F_0 \sin^4(\pi t/T)$ for the rest of the pulse. For such a pulse, the effective interaction time is given by [25]

$$T_{\rm eff}^{(M)} = \frac{(4M-1)!!}{(4M)!!}2t_{\rm cr} + \frac{T}{2^{M-2}\pi}\sum_k^{2M-1}(-1)^k\frac{(4M)!}{(4M-k)!k!}\frac{\sin[(4M-2k)\pi t_{\rm cr}/T]}{M-2k}\,. \tag{29}$$

Even if the ionization channel is only closed in a very narrow time window close to the peak intensity, the effective pulse duration will be significantly smaller than the pulse duration and, of course, also much smaller than the effective interaction time in the absence of channel closing given by equation (27). This is especially the case for processes of intermediate to high order. Finally, we note that the bandwidth of the source, $\Delta\omega = 2\pi/T$, may be of the same order as ΔE or $U_{\rm P}$ for 50 fs pulses. This means, that the effective interaction time, in the case of channel closing, is not generally as clearly defined as above.

The present method of determining generalized cross-sections applies to all atoms and molecules for which an efficient solution of the TDSE is possible. Closing this section, we note that the analysis proposed here can be used to study experimental photoelectron energy spectra. The method will then directly give the ratio between the generalized cross-sections, $\hat\sigma_{N+1}/\hat\sigma_N$ etc.

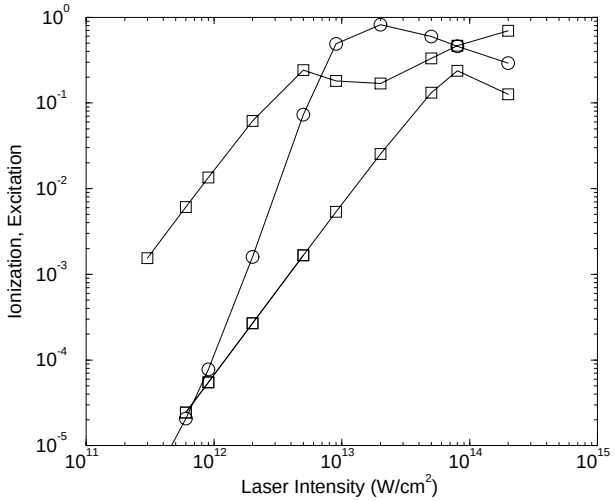

Fig. 1. Ionization yields for a 50 fs pulse at 355 nm in Ps (upper curve) and for a 25 fs pulse at 177.5 nm in H (lower curve). The circles show the total population in the excited states of Ps.

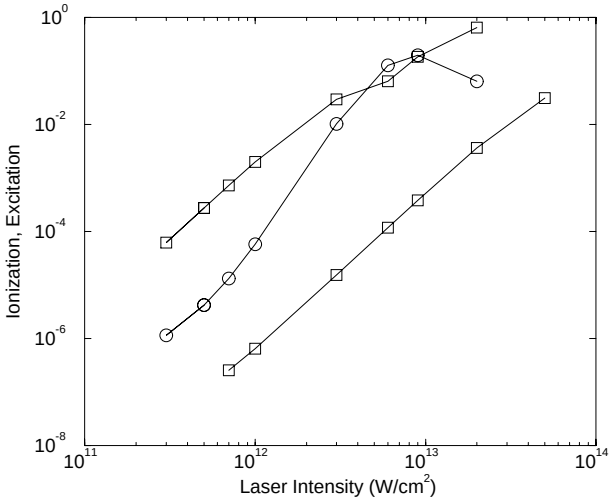

Fig. 2. Ionization yields for a 50 fs pulse at 532 nm in Ps (upper curve) and for a 25 fs pulse at 266 nm in H (lower curve). The circles show the total population in the excited states of Ps.

5 Results and discussion

In this section, we present and discuss the results of non-perturbative TD calculations of Ps (and H) under strong subpicosecond fields. We also present results of generalized cross-sections and photoelectron energy spectra obtained by the rate equation method of Section 4. The calculations have been performed in the two-, three- and six-photon ionization regimes of Ps at wavelengths of $\lambda = 355$, 532 and 1064 nm, corresponding to photon energies of $\hbar\omega = 3.49$, 2.33 and 1.17 eV, respectively. These cases correspond to situations where Ps absorbs an excess energy of only $\Delta E = 0.18{-}0.19$ eV above the threshold against photobreakup ($E_\infty^{(\mathrm{Ps})} = 6.8$ eV) and are at the wavelengths which are accessible in the laboratory in Aarhus [13]. Additionally, we have performed calculations at the wavelength of the Ti:sapphire laser, $\lambda = 780$ nm ($\hbar\omega = 1.59$ eV), which corresponds to the five-photon ionization regime of Ps.

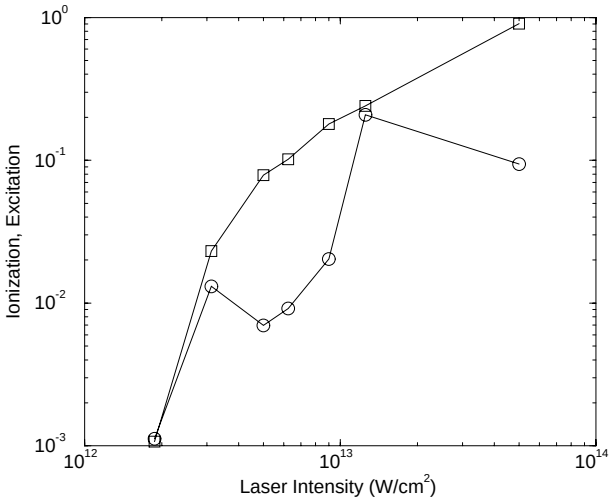

Fig. 3. Ionization yields for a 50 fs pulse at 780 nm in Ps. The circles show the total population in the excited states of Ps.

5.1 Photobreakup yields

Figures 1–4 show ionization (photobreakup) yields of Ps as a function of intensity in the two-, three-, five-, and six-photon ionization regimes at the wavelengths detailed in the captions for a 50 fs laser pulse. Also shown in the figures, is the total excitation of Ps and finally, in Figures 1 and 2, also the ionization yield in H at appropriately scaled pulse duration and frequency, as discussed in Section 3. The general trend is as expected: the ionization yield increases with intensity. There are, however, a few points which deserve more detailed discussion.

In Figures 1 and 2, the upper and lower curves labeled by squares are the yields in Ps and H, respectively. As discussed in Section 3, in the perturbative regime, the yields for H coincide with the yields for Ps if the former are multiplied by a factor of 2^{4N} (see Eq. (17)), where N is the order of the process (2 or 3 in this case). It is verified, that the yields for Ps and H for the 3 lowest intensities in Figure 1, with the scaling of the hydrogenic values by a factor of 2^8, will be essentially on top of each other. A small deviation sets in at an intensity of 2×10^{12} and at 5×10^{12} W/cm^2 where the yield of Ps differs substantially from the LOPT result obtained by scaling the yield in H. Similarly, in Figure 2 in the three-photon ionization regime, the yields compare well through scaling (2^{12}) up to intensities $\sim 10^{12}$ W/cm^2. The ionization yield curve in Figure 1 shows a significant effect of channel closing. As the peak intensity is increased to $\sim 7{-}8 \times 10^{12}$ W/cm^2, the AC Stark shift of the threshold (the ponderomotive potential) becomes so large that the two-photon ionization channel closes and 3 photons are needed to overcome the barrier against ionization (see Tab. 1 for the ponderomotive shifts). The closing of the channel means that the

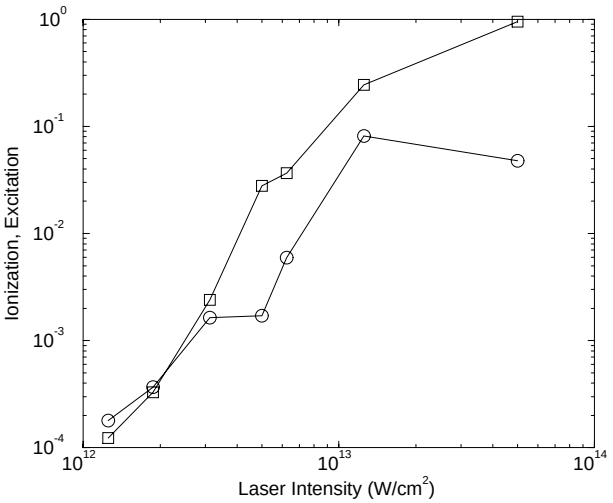

Fig. 4. Ionization yields for a 50 fs pulse at 1064 nm in Ps. The circles show the total population in excited states of Ps.

saturation intensity is reached at an intensity more than one order of magnitude higher than expected from a (guided by the eye) continuation of the lower part of the ionization yield curve. We note from the figure, that a similar non-monotonic behavior of the ionization yield is observed in H, but at an intensity $2^4 = 16$ times larger than in Ps, in accordance with the rigorous scaling rule of equation (13) (see also Ref. [3]). In Figure 2 the three-photon ionization channel closes at an intensity of $\sim 3{-}4 \times 10^{12}$ W/cm^2, but the effect on the ionization yield is less dramatic than in Figure 1. This it partly due to the difference in the photon energy in the two cases: the smaller the photon energy is, the easier it is to absorb an extra photon; but it is also related to the difference in the excitation of Ps shown in the two figures. In Figure 1, there is a surprising and interesting efficient excitation of Ps over a wide range of intensities ($\sim 7 \times 10^{12}{-}8 \times 10^{13}$ W/cm^2). Up to $\sim$ 80% may be found in excited states after the pulse. In Figure 2, the excitation is somewhat less (up to $\sim$ 20%) and restricted to a narrower range of intensities ($\sim 5{\times}10^{12}{-}10^{13}$ W/cm^2). In both cases, the population of excited states is due to resonant population transfer. The distribution of population in principal quantum numbers is rather broad in this regime, as the whole Rydberg series scans through the virtual level corresponding to two- and three-photon absorption, respectively. Specifically, the excited states keeping most of the population are $n = 3{-}6$ at 355 nm and $n = 4{-}7$ at 532 nm. In accordance with parity conservation, it is mainly the s and d states that are excited at 355 nm while it is the p and f states at 532 nm. The reason that the population of the excited states of Ps is smaller at 532 than at 355 nm, is that the effective three-photon coupling is smaller than the coupling for the two-photon transition at the intensity where the excited states move into resonance.

The potential usefulness of this high excitation lies in the charge exchange with antiprotons for the production of antihydrogen (since the charge-transfer cross-section increases quite rapidly with the excitation (n) and the angular momentum [15]), as well as in the spectroscopy of excited states. The efficient few-photon excitation mechanism by pulses of short duration has been discussed in more detail in reference [4], including an analysis of the population in partial waves.

Figure 3 shows the ionization yield for a 50 fs pulse and wavelength of 780 nm, corresponding to a photon energy of 1.59 eV. The absorption of 5 photons leads to an excess energy of 1.15 eV. From the value of $U_{\rm P}$ in Table 1, we do not expect any channel closing at intensities below $\sim 9 \times 10^{12}$ W/cm^2. The line between the first two ionization yields in the figure has a slope very close to 5, and thus up to $\sim 3 \times 10^{12}$ W/cm^2 it is in the perturbative regime. Even though the excitation is comparable with the ionization yield, it is still so small that it can be neglected and the method of Section 4 for the determination of the generalized cross-sections in Table 2 can be applied in this regime. At intensities above $\sim 3 \times 10^{12}$ W/cm^2, LOPT breaks down and the ionization yield has to be predicted by the nonperturbative method.

The excitation has some structures which can be understood in terms of AC Stark shifts. At an intensity of $\sim 3 \times 10^{12}$ W/cm^2, the $n = 3$ level of Ps is shifted into four-photon resonance and the $3s$ and the $3d$ states have all of the excited state population. As the intensity is increased further, the resonance condition is no longer fulfilled and the excited state population drops. At an intensity of 1.25×10^{13} W/cm^2, the excited state population is high again ($\sim$ 20%). At this intensity the shift of the threshold is so large that the five-photon ionization channel has been significantly influenced by channel closing and 6 photons are needed to ionize. In fact, the states with principal quantum number $n = 4{-}6$ have moved into five-photon resonance; hence the peak in the excitation population. Notice, that the Keldysh parameter (Tab. 1) approaches unity for the higher intensities in Figure 3 which signals the transition from the multiphoton into the tunneling regime.

By comparison with Figures 1 and 2, we see that a channel closing is consistently accompanied by an increase in the excited state population. This is due to the shifting of the Rydberg series through the virtual level corresponding to N-photon absorption ($N = 2$, 3 and 5 in this case).

In the six-photon ionization regime, we have considered the wavelength of 1064 nm which corresponds to a photon energy of $\hbar\omega = 1.17$ eV and an excess energy of 0.19 eV. Figure 4 shows the ionization yield and the excitation in Ps in this regime. Due to the rather high-order of the process, many states are now shifting in and out of resonance and, accordingly, the population in excited states as a function of principal quantum number and angular momentum up to $l = 4$ is distributed rather broadly and homogeneously. Not much population is found in states with angular momentum larger than $l = 4$. The Keldysh parameter is larger than unity for intensities smaller than 1.6×10^{13} W/cm^2. Up to about 10% of the total population can be found in excited states after the short pulse. As suggested by the value of $U_{\rm P}$ in Table 1, the six-photon ionization channel is already influenced by channel closing

Table 2. Generalized cross-sections in the two-, three-, five- and six-photon ionization regimes for H and Ps. The cross-sections in the two-, three- and five-photon ionization regimes have been extracted with the method described in Section 4. In the six-photon ionization regime the values for the hydrogenic generalized cross-sections have been taken from the literature [23,24] and the results for Ps are obtained through scaling [3].

$N+S$	$\lambda^{(\mathrm{H})}$(nm)	$\lambda^{(\mathrm{Ps})}$(nm)	$\hat{\sigma}^{(\mathrm{H})}_{N+S}\left(\frac{\mathrm{cm}^{2(N+S)}}{\mathrm{S}^{N+S-1}}\right)$	$\hat{\sigma}^{(\mathrm{Ps})}_{N+S}\left(\frac{\mathrm{cm}^{2(N+S)}}{\mathrm{S}^{N+S-1}}\right)$
$2+0$	177.5	355	1×10^{-50}	4×10^{-49}
$2+1$	177.5	355	3×10^{-84}	8×10^{-82}
$2+2$	177.5	355	7×10^{-118}	2×10^{-114}
$2+3$	177.5	355	2×10^{-151}	3×10^{-147}
$3+0$	266	532	4×10^{-83}	1×10^{-80}
$3+1$	266	532	8×10^{-116}	2×10^{-112}
$3+2$	266	532	6×10^{-149}	1×10^{-144}
$3+3$	266	532	9×10^{-182}	1×10^{-176}
$5+0$	390	780	3×10^{-148}	5×10^{-144}
$5+1$	390	780	4×10^{-181}	6×10^{-176}
$5+2$	390	780	5×10^{-214}	6×10^{-208}
$5+3$	390	780	7×10^{-248}	6×10^{-241}
$6+0$	530	1060	4×10^{-180}	5×10^{-175}
$6+1$	530	1060	3×10^{-212}	3×10^{-206}
$6+2$	530	1060	1×10^{-244}	1×10^{-237}
$6+3$	530	1060	4×10^{-277}	3×10^{-269}
$6+4$	530	1060	1×10^{-309}	8×10^{-301}
$6+5$	530	1060	5×10^{-342}	2×10^{-332}

at intensities around $8-9\times10^{11}$ W/cm^2. In the low intensity limit of Figure 4, we see that the slope is much lower than 6 which would be the value predicted by LOPT. This is because excited states are now populated during the pulse and the ionization takes place from these, causing a lower slope. A similar behavior has been found theoretically in potassium and hydrogen by Maragakis *et al.* [26], in agreement with experimental findings by Sheehy *et al.* [27]. The method discussed in Section 4.2 for the extraction of the generalized cross-sections can not be applied when the perturbative regime is not clearly identified. In Table 2, we nevertheless present results in the six-photon ionization regime at wavelengths of 530 and 1060 nm for H and Ps, respectively. The hydrogenic values are taken from the literature [23,24] and the values for Ps are obtained through scaling (Sect. 3 and Ref. [3]).

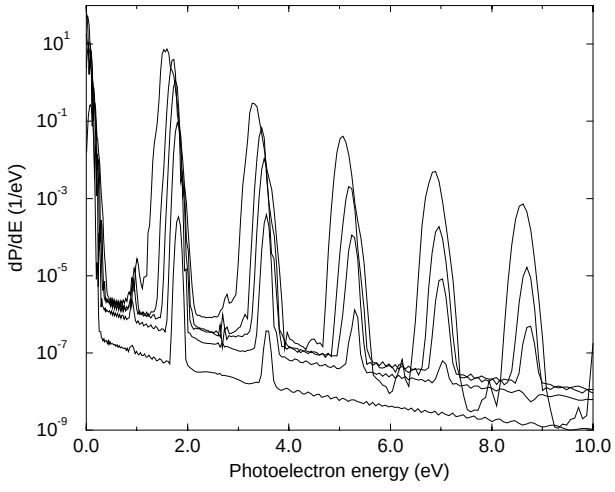

Fig. 5. Photoelectron spectrum of Ps for a 50 fs pulse at 355 nm (two-photon ionization regime). The intensities are 3×10^{11}, 2×10^{12}, 5×10^{12}, 9×10^{12} and 2×10^{13} W/cm^2 from the lower to the upper curve.

5.2 Photoelectron energy spectra for 50 fs pulses

Figures 5–8 show the photoelectron energy spectra of Ps for a 50 fs laser pulse for a selection of laser intensities at wavelengths of 355, 532, 780 and 1064 nm, corresponding to the two-, three-, five-, and six-photon ionization regimes. The energy separation between adjacent peaks is $\hbar\omega/2$ due to the equal energy sharing between the electron and the positron in the center of mass system with Ps initially at rest. As the intensity is increased the absorption of excess photons becomes more likely. Simultaneously, the peaks move to the left due to the laser-induced upward shift of the threshold. Note that the static polarizability of Ps is 8 times larger than the

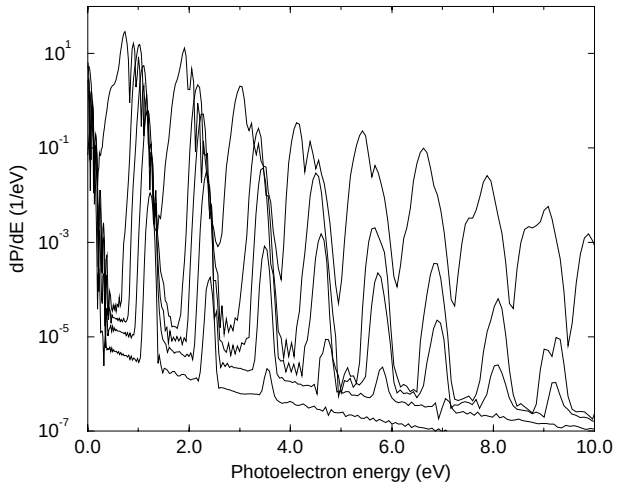

Fig. 6. Photoelectron spectrum of Ps for a 50 fs pulse at 532 nm (three-photon ionization regime). The intensities are 1×10^{12}, 3×10^{12}, 6×10^{12}, 9×10^{12} and 2×10^{13} W/cm^2 from the lower to the upper curve.

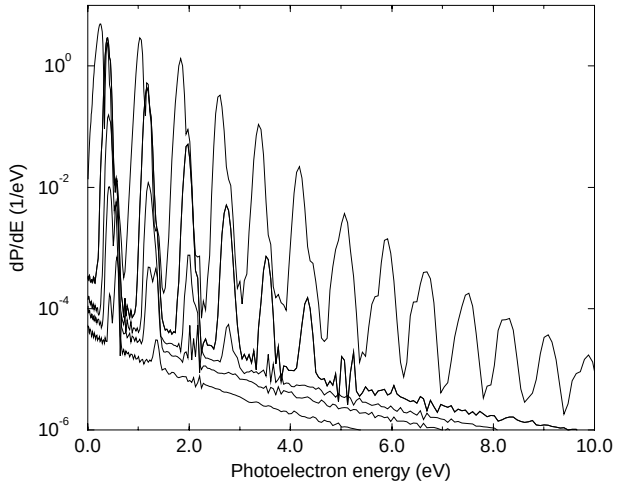

Fig. 7. Photoelectron spectrum of Ps for a 50 fs pulse at 780 nm (five-photon ionization regime). The intensities are 6.25×10^{11}, 1.25×10^{12}, 1.875×10^{12}, 3.125×10^{12}, and 6.25×10^{12} W/cm^2 from the lower to the upper curve.

one in H [3]. The shift of the ground state is therefore often essential in interpreting the TD results, by calculating the shifts with second order perturbation theory [4].

Comparing the relative height between the first and the second peak of the ATI-spectrum in Figures 5, 6 and 8, where, in all cases, we ionize just above the threshold *via* the lowest channel, we note a more pronounced effect of channel closing, as more photons are required to reach the threshold. This is because the AC Stark shift of the threshold is proportional to ω^{-2}. In fact, in Figure 8 the photoelectron energy spectrum is already influenced by channel closing at the lowest intensity in the figure. In Figure 7, we are well above the threshold in the five-photon ionization channel (1.15 eV) and almost no effects of channel closing are noticeable in the figure. At the highest intensity

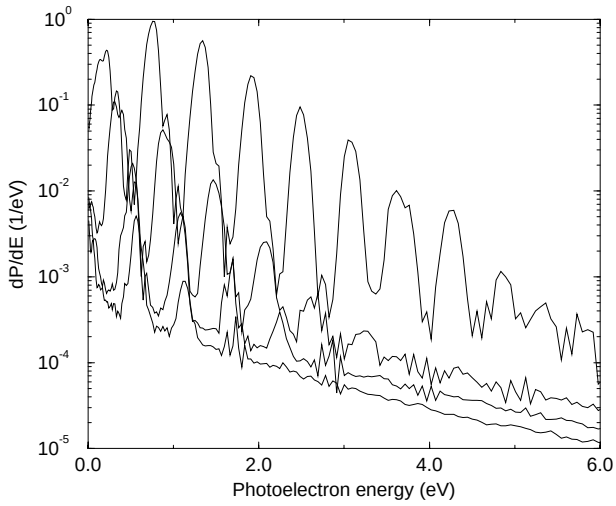

Fig. 8. Photoelectron spectrum of Ps for a 50 fs pulse at 1064 nm (five-photon ionization regime). The intensities are 1.25×10^{12}, 1.875×10^{12}, 3.125×10^{12}, and 5×10^{12} from the lower to the upper curve.

in the figure, the relative height between successive peaks is about 2 for the 3 first peaks.

In Figure 5 there is a peculiarity. At photoelectron energies of $\sim$ 0.9 and $\sim$ 2.7 eV we see small side peaks. These are due to an off-resonant one-photon coupling between the $1s$ and $2p$ bound states. The peaks correspond to one- and two-photon ionization from the $2p$-level. The relative height between the first peak ($S = 0$) and the one-photon ionization signal from the $2p$ level is consistent with the ratio between the Rabi frequency and the detuning, as it would be in a simple two-state model of this restricted part of the Hilbert space. Similar substructures have been observed experimentally in few-photon ionization of cesium with 70 fs pulses [28].

In Figures 7 and 8, the values of the outermost peaks at the highest intensity have to be viewed with some reservation since only 14 angular momenta have been included, as it was not practical to do the calculation for more states.

Figure 9 shows scaling of the photoelectron energy peaks in the perturbative regime of two-photon ionization (see Figs. 1 and 5). We see, that the heights of the ATI peaks in Ps can be obtained from the corresponding peaks in H through multiplication by the appropriate factor, as given in the caption and as calculated from equation (18) of Section 3. Thus, Figure 9 can reveal whether a calculation is in the perturbative regime or not. A result of the sort presented in Figure 9 also provides a very delicate check to the accuracy of the present code used for the TD calculations.

5.3 Photoelectron energy spectra for nanosecond pulses

As discussed in Sections 1 and 4, the TD method becomes impossible to use for pulses of durations of the order of nanoseconds. One alternative method is to estimate

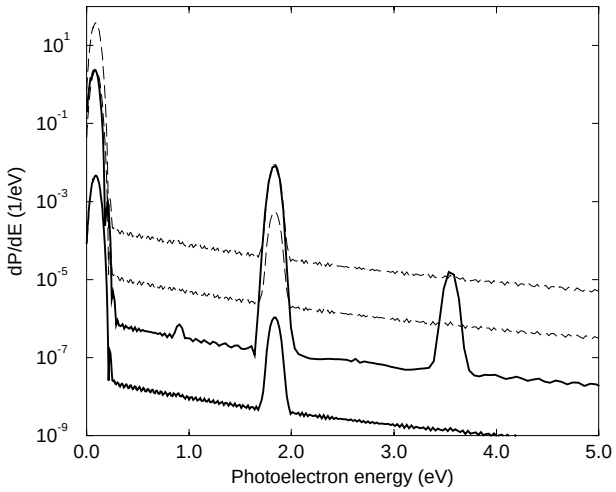

Fig. 9. Photoelectron energy spectrum of Ps for a 50 fs pulse in the two-photon ionization regime at 355 nm (upper bold curve), and for H for a 25 fs pulse at the scaled wavelength 177.5 nm (lower bold curve), both for an intensity of 9×10^{11} W/cm^2. The upper dashed curve is the lower full curve for H multiplied by 2^{13}, the lower dashed curve is the lower full curve for H multiplied by 2^9. The photoelectron energy in the photoelectron spectra for H are multiplied by a factor of 1/4 to make a direct comparison with the Ps results possible.

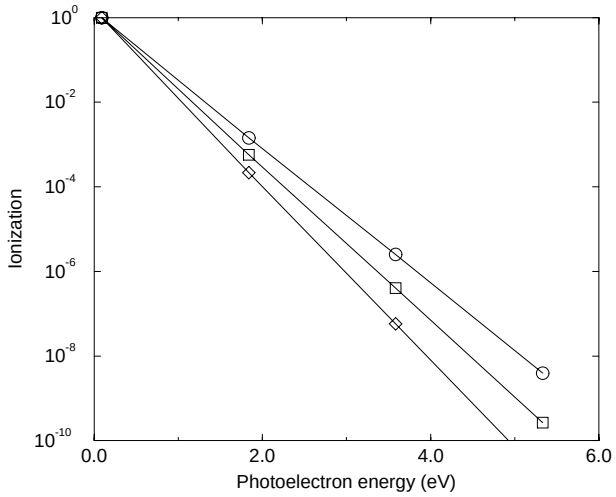

Fig. 10. Ionization yields for pulse lengths of 0.1 (circles), 1 (squares), and 10 ns (diamonds) as a function of the photoelectron energy in the two-photon ionization regime of Ps ($\lambda = 355$ nm). The laser intensity is 9×10^{11} W/cm^2. The lines in the figure have no physical meaning.

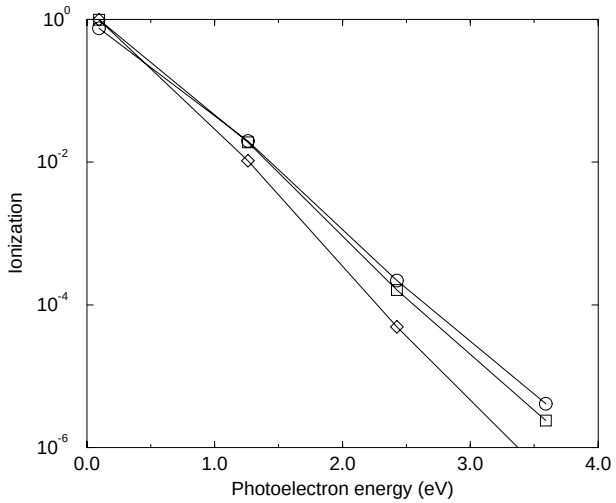

Fig. 11. Ionization yields for pulse lengths of 0.1 (circles), 1 (squares), and 10 ns (diamonds) as a function of the photoelectron energy in the three-photon ionization regime of Ps ($\lambda = 532$ nm). The laser intensity is 7×10^{11} W/cm^2. The lines in the figure have no physical meaning.

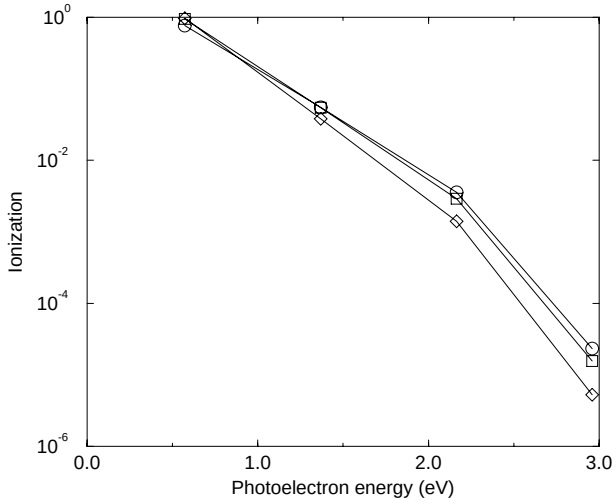

Fig. 12. Ionization yields for pulse lengths of 0.1 (circles), 1 (squares), and 10 ns (diamonds) as a function of the photoelectron energy in the five-photon ionization regime of Ps ($\lambda = 780$ nm). The laser intensity is 1.8×10^{12} W/cm^2. The lines in the figure have no physical meaning.

the photoelectron energy spectrum from a perturbative calculation solving the rate equations of Section 4.1, after having extracted generalized cross-sections with the method described in Section 4.2. The values we have used for the generalized cross-sections are presented in Table 2. Figures 10–13 show partial ionization yields for 3 different pulse lengths (0.1, 1 and 10 ns) at intensities in the perturbative regime and in different multiphoton ionization regimes. Note that, the shorter the pulse is, the larger the signal in the higher-order channels. This is because the system now has less time to ionize *via* the lowest order channel: at the maximum intensity there will still be a fair percentage of neutral atoms left to ionize.

From the relative height of the yields in Figure 10, we conclude that 2 photoelectron energy peaks should be observable in the two-photon ionization regime with a standard resolution (~ 4 orders of magnitude) for strong field experiments and for the pulse durations in the contemplated experiment [13]. From Figure 11 we conclude that probably three ATI peaks could be measured in an experiment using the laser parameters in the figure.

Figure 12 shows the partial ionization yields in the five-photon ionization regime. As discussed above, the value

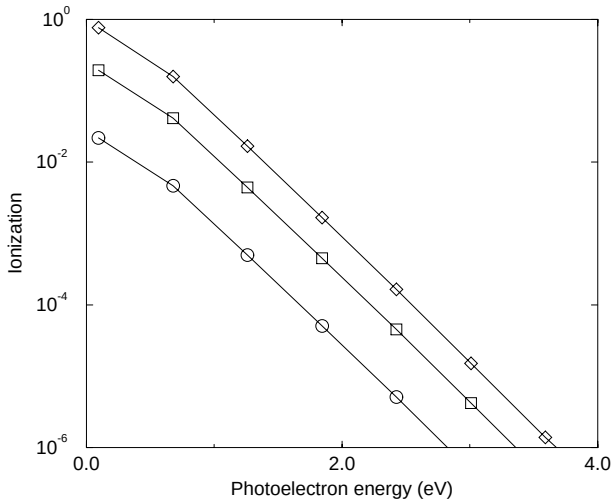

Fig. 13. Ionization yields for pulse lengths of 0.1 (circles), 1 (squares), and 10 ns (diamonds) as a function of the photoelectron energy in the six-photon ionization regime of Ps ($\lambda = 1064$ nm). The laser intensity is 7×10^{11} W/cm^2. The lines in the figure have no physical meaning.

of the generalized cross-section corresponding to a photobreakup process with the absorption of $5+3$ photons and a photoelectron energy of 2.96 eV is somewhat uncertain and at the lower side of the true value. We see therefore a drop in the signal at this energy. For the intensity in the figure, 3 or possibly 4 photoelectron energy peaks can be resolved experimentally.

Figure 13 shows the yields at the photoelectron energies in the channels corresponding to the absorption of $S = 0{-}6$ photons above the $N = 6$ photon ionization threshold. The generalized cross-sections are, in this case, taken from the literature [23,24]. By comparison with the similar figures in the two-, three- and five-photon ionization regimes, we see that the process of the higher order favors transitions in the continuum. Up to 5 peaks are expected to be seen in an experiment at this wavelength, intensity and for the pulse durations considered. We have used an intensity of 7×10^{11} W/cm^2 which we expect to be low enough to make a description in terms of LOPT accurate for the long pulse. The intensity is so low that no effect of channel closing is expected (see the value of $U_{\rm P}$ in Tab. 1).

6 Summary and conclusion

We have presented a compilation of results for Ps in strong laser fields across the two-, three-, five- and six-photon ionization regimes. We have adopted a nonperturbative approach by solving the TDSE in a discretized basis. Using this method, we have calculated ionization yields and photoelectron energy spectra and compared some of our results (through a rigorous scaling law) with results in H. The purpose of this was to (i) shed some light on the differences in the response to an intense laser field between Ps and H and (ii) provide a very sensitive and reliable check of our numerics. It was shown that the interaction of Ps with a strong pulse of short duration can serve as an efficient excitation mechanism. In the two-photon ionization case as much as 80% of the population can be transferred to excited states, in the three-photon ionization regime 20% can be promoted while in the five- and six-photon ionization regimes 10–20% of the population can be found in excited states after the subpicosecond pulse. The effective transfer is connected with AC Stark shifts, closing of ionization channels and states shifting into resonance during the pulse.

The TD method is practical for pulses in the subpicosecond regime. For longer pulses this method imposes very high demands on computational speed and memory. These demands can not be met by present day computers and it is therefore not a fruitful avenue. Alternative methods are therefore needed for the prediction of the outcome of experiments in the nanosecond regime. One such approach is the solution of the rate equations including ATI as discussed here. Importantly, we have also outlined a method which allows one to derive the relevant values of the generalized cross-section from the nonperturbative TD calculation. Another method, not discussed here, which allows the prediction of ionization rates and generalized cross-sections in the long-pulse-duration domain relies on the Floquet approach but in this case the only quantity which is readily obtained is the total ionization width and a delicate renormalization procedure has to be adopted if partial rates are needed (see, *e.g.* the discussion by Potvliege and Shakeshaft in Ref. [29]). Also the "long" nanosecond pulses favor the perturbative approach, in the sense that much of the ionization dynamics will occur during the rise of the pulse at intensities where the atomic response to the field is perturbative.

Discussions with Peter Balling and Merete Raarup on the experimental details of the positronium experiment in Aarhus are gratefully acknowledged. L.B.M. acknowledges support from the Danish Natural Science Research Council (Grant. No. 9800755).

References

1. E.M. Karule, *Atomic Processes, Report of the Letvian Academy of Sciences* (In Russian, Unpublished, Riga, 1975).
2. Y. Gontier, M. Trahin, Phys. Rev. A **4**, 1896 (1971).
3. L.B. Madsen, P. Lambropoulos, Phys. Rev. A **59**, 4574 (1999).
4. L.B. Madsen, L.A.A. Nikolopoulos, P. Lambropoulos, J. Phys. B: At. Mol. Opt. Phys. **32**, L425 (1999).
5. L.B. Madsen, L.A.A. Nikolopoulos, P. Lambropoulos, Hyperf. Interact. (in press).
6. A. Rich, Rev. Mod. Phys. **53**, 127 (1981).
7. A.P. Mills Jr, S. Chu, in *Quantum Electrodynamics*, edited by T. Kinoshita (World Scientific, Singapore, 1990).
8. M.S. Fee, A.P. Mills Jr, S. Chu, E.D. Shaw, K. Danzmann, R.J. Chichester, D.M. Zuckerman, Phys. Rev. Lett. **70**, 1397 (1993).

9. M.S. Fee, S. Chu, A.P. Mills Jr, R.J. Chichester, D.M. Zuckerman, E.D. Shaw, K. Danzmann, Phys. Rev. A **48**, 192 (1993).
10. M.H. Holzscheiter, M. Charlton, Rep. Prog. Phys. **62**, 1 (1999).
11. G. Baur, G. Boero, S. Brauksiepe, A. Buzzo, W. Eyrich, R. Geyer, D. Grzonka, J. Hauffe, K. Kilian, M. LoVetere, M. Macri, M. Moosburger, R. Nellen, W. Oelert, S. Passaggio, A. Pozzo, K. Roehrich, K. Sachs, G. Schepers, T. Sefzick, R.S. Simon, S. Stratmann, F. Stinzing, M. Wolke, Phys. Lett. B **368**, 251 (1996).
12. G. Blanford, D.C. Christian, K. Gollwitzer, M. Mandelkern, C.T. Munger, J. Schultz, G. Zioulas, Phys. Rev. Lett. **80**, 3037 (1998).
13. P. Balling, J. Merrison, M.K. Raarup (private communication).
14. H.A. Bethe, E.E. Salpeter, *Quantum Mechanics of One- and Two-Electron Atoms* (Springer-Verlag, Berlin-Göttingen-Heidelberg, 1957).
15. J. Mitroy, Phys. Rev. A **52**, 2859 (1995).
16. T.N. Chang, *B-spline based Configuration-Interaction Approach for Photoionization of Two-electron and Divalent Atoms in Many-Body Theory of Atomic tructure* (World Scientific, Singapore, 1993).
17. J. Sapirstein, W.R. Johnson, J. Phys. B: At. Mol. Opt. Phys. **29**, 5213 (1996).
18. P. Lambropoulos, P. Maragakis, J. Zhang, Phys. Rep. **305**, 203 (1998).
19. J. Zhang, P. Lambropoulos, J. Phys. B: At. Mol. Opt. Phys. **28**, L101 (1995).
20. E. Cormier, P. Lambropoulos, J. Phys. B: At. Mol. Opt. Phys. **30**, 77 (1997).
21. H. Friedrich, in *Atoms and molecules in strong external fields*, edited by P. Schmelcher, W. Schweizer (Plenum, New York, 1998).
22. P. Lambropoulos, X. Tang, J. Opt. Soc. Am. B **4**, 821 (1987).
23. Y. Gontier, M. Trahin, J. Phys. B **13**, 4383 (1980).
24. F.H.M. Faisal, *Theory of Multiphoton Processes* (Plenum, New York, 1987).
25. I.S. Gradsteyn, I.M. Ryznik, in *Table of Integrals, Series, and Products*, edited by A. Jeffrey (Academic Press Inc., San Diego, 1965).
26. P. Maragakis, E. Cormier, P. Lambropoulos, Phys. Rev. A **60**, 4718 (1999).
27. B. Sheehy, P. Agostini, L.F. DiMauro, Phys. Rev. Lett. (in press).
28. W. Nicklich, H. Kumpfmüller, H. Walther, X. Tang, Haule Xu, P. Lambropoulos, Phys. Rev. Lett. **69**, 3455 (1992).
29. R.M. Potvliege, R. Shakeshaft, in *Atoms in Intense Laser Fields*, edited by M. Gavrila (Academic, Boston, 1992), p. 373.